Exploring the Archives: A Search for Novae in UVIT Snapshots of M31

Basu et al. 2024,APJ,917:8

Reporter: Yu Pan

2024/09/14

OUTLINE

Introduction

The importance of studying novae

- Novae are cataclysmic events triggered by thermonuclear runaway reactions on the surface of accreting white dwarfs.
- These novae eruptions increase the brightness of the binary system up to several orders of magnitude, triggering nucleosynthesis and expelling material into the interstellar medium.
- Individual novae are excellent laboratories for understanding accretion and mixing processes, binary evolution, supernova type Ia progenitors, and shock mechanisms. Nova studies are also important tracers of galactic chemical evolution and ISM enrichment.

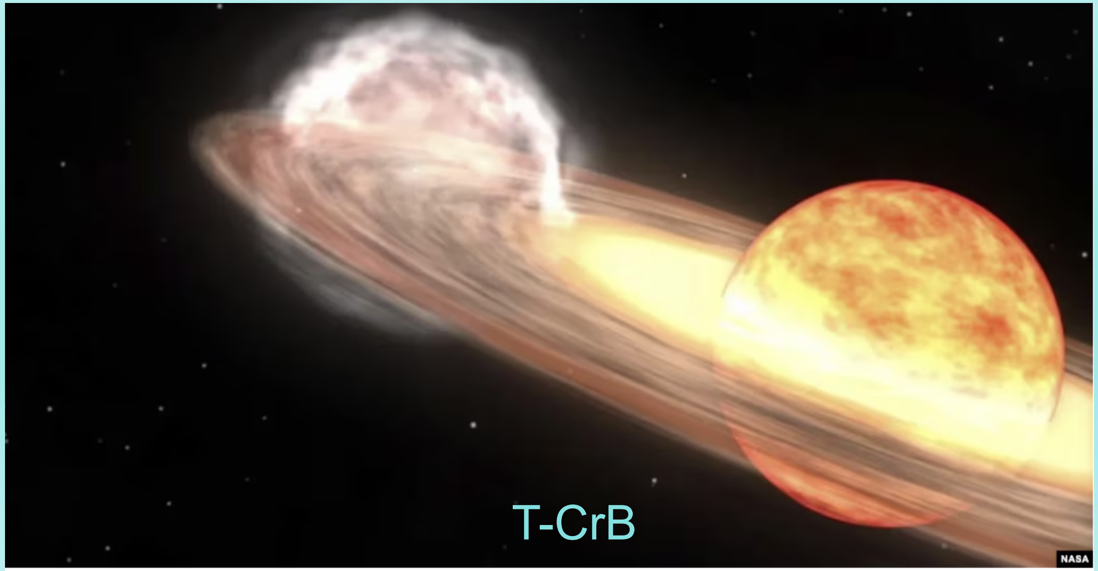

Introduction

Why study novae in M31

- One of the galaxies in which novae are studied in detail is M31, owing to its full visibility for more than half a year, close distance, low inclination, and high nova rate.
- High occurrences of recurrent novae (RNe) in M31, particularly those with short recurrence periods of fewer than 10 yr.

Why UV?

- Rare UV studies of extragalactic novae, such as that of Cao et al. (2012) for M31, and those of Lessing et al. (2023) and Shara et al. (2023) for M87, concentrated primarily on eruption characteristics, spatial distribution, nova rates, and population studies.
- Nonetheless, no study has been reported in the literature honing in on the systematic study of the quiescence phase of extragalactic novae in the UV.

DATA

Introduce the telescope

- AstroSat is a space-based high-energy telescope in a low-inclination Earth orbit.
- UVIT is one of the primary instruments on board AstroSat, consisting of a twin telescope with one FUV (130-180 nm) and one NUV(180-300 nm)/visible (320-550 nm) channel, capable of observing simultaneously.
- Both telescopes have a mirror of 38 cm diameter and a circular field of view of 28′. UVIT has one of the best spatial resolutions at 1.5” in the UV.
- UVIT’s FUV filters offer a unique wave band (up to 1000 Å) to detect and study novae.

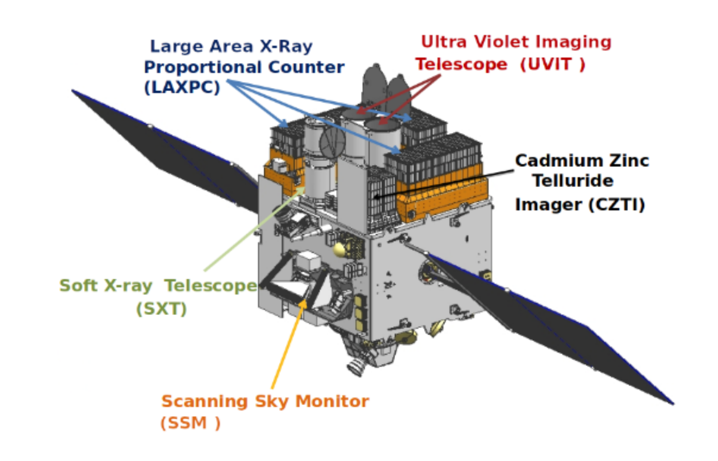

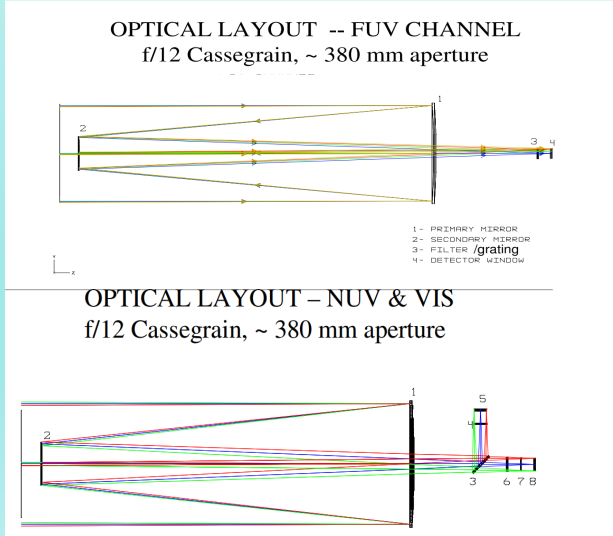

https://astrobrowse.issdc.gov.in/astro_archive/archive/Home.jsp

DATA

Leahy et al. 2021

UVIT has observed multiple fields of M31 in different filters over multiple epochs.

- Sky locations of the fields for the UVIT survey of M31, showing the field of view for the fields, labeled F1 to F19 in black.

- The background image is the DSS Poss2 blue filter image of M31. The white ellipse shows the size of the D25 ellipse for M31, from Gil de Paz et al. (2007).

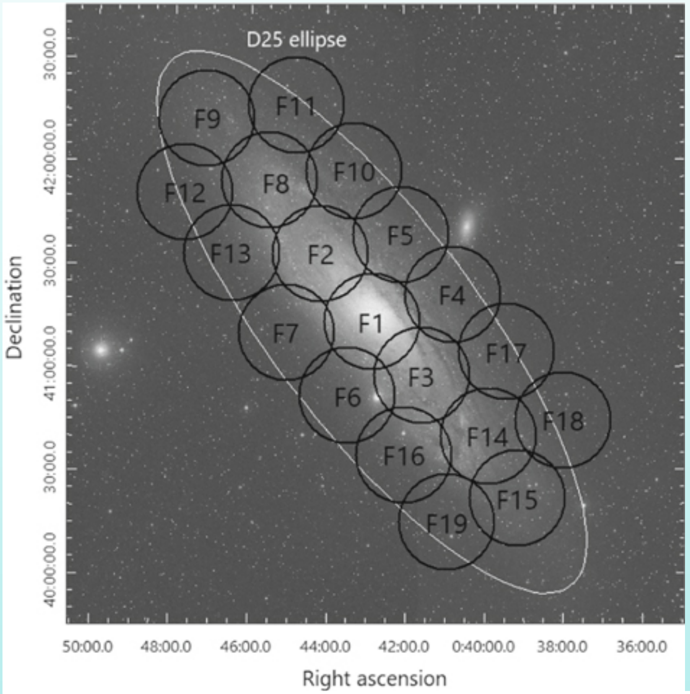

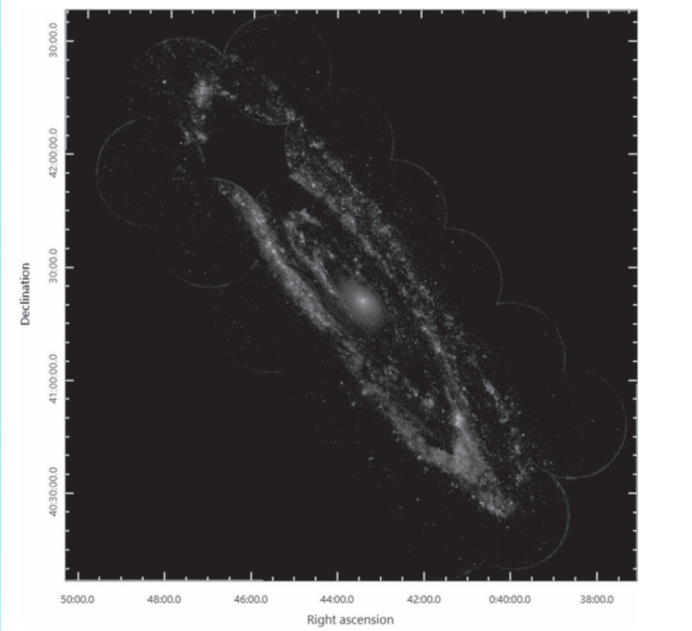

DATA

2.1. Observations and Data Reduction

- They processed the data using CCDLAB (Postma & Leahy 2017). The automated steps in CCDLAB include flat-fielding, drift correction, and cosmic-ray correction. (All the data utilized in this work have been summarized in Table 1)
- The orbit-wise images were registered and merged to get a single image with a high signal-to-noise ratio. The final step in CCDLAB involved performing astrometry on the merged and orbit-wise images.
- Individual images were normalized by their exposure times to bring them to the same scale. The normalized images were then tiled using Swarp. The exposure array frames generated by CCDLAB were used as weights to take care of the edges and overlapping regions during tiling. The M31 FUV mosaic is shown in Figure 1.

Table 1
UVIT Observation Log of All Images, Including Coadded Frames, in Which at Least One Nova Was Detected

Observation ID	R.A. (deg)	Decl. (deg)	Filter	Field	Obs Epoch (BJD)	Exp Time (s)	Limiting Mag (AB mag)	Novae Detected
A02_028T01_9000000724	10.71683	41.12430	F148W	M31 01	2457671.85662	7736.347	22.94	18
A02_028T01_9000000724	10.71683	41.12430	F172M	M31 01	2457672.19496	3611.883	21.39	14
A02_028T01_9000000724	10.71683	41.12430	N219M	M31 01	2457671.85657	7780.686	22.08	12
A02_028T01_9000000724	10.71683	41.12430	N279N	M31 01	2457672.19491	3627.438	21.53	11
A07_007T04_9000003310	10.70412	41.27929	F148W	M31 01	2458805.25645	17045.731	23.37	17
A07_007T04_9000003310	10.70412	41.27929	F169M	M31 01	2458804.85075	10426.754	22.63	15
A07_007T04_9000003310	10.70412	41.27929	F172M	M31 01	2458806.27133	16606.192	22.34	15
A10_002T04_9000004022	10.59843	41.21609	F148W	M31 01	2459174.71396	11759.864	23.10	18
A02_028T03_9000000788	11.01776	41.54606	F148W	M31 02	2457704.13548	7942.829	22.69	3
A02_028T03_9000000788	11.01776	41.54606	F172M	M31 02	2457704.48574	5350.934	21.48	2
A02_028T03_9000000788	11.01776	41.54606	N219M	M31 02	2457704.13543	7986.231	22.01	2
A02_028T03_9000000788	11.01776	41.54606	N279N	M31 02	2457704.48567	5544.727	21.33	3
A10_002T05_9000004000	11.13728	41.48918	F148W	M31 02	2459167.97966	12610.195	22.77	1
A04_022T02_9000002184	11.33933	41.88125	F148W	M31 08	2458292.30948	3371.811	22.85	1
A04_022T02_9000002184	11.33933	41.88125	F172M	M31 08	2458292.98608	9017.513	22.29	1
A05_004T03_9000002508	9.87699	40.36606	F148W	M31 15	2458435.07551	4610.422	23.04	1
A05_004T03_9000002508	9.87699	40.36606	F169M	M31 15	2458435.27774	9286.96	22.69	1
A05_004T03_9000002538	9.86651	40.37805	F148W	M31 15	2458449.21674	2104.392	22.72	1
A05_004T03_9000002538	9.86651	40.37805	F169M	M31 15	2458449.42980	9224.752	22.76	1
Coadded frames[a]	10.70959[b]	41.27957[b]	F148W	M31 01	2458550.60901[c]	36541.942	23.54	3[d]
Coadded frames[a]	10.70959[b]	41.27957[b]	F172M	M31 01	2458239.23315[c]	20218.075	22.50	1[d]

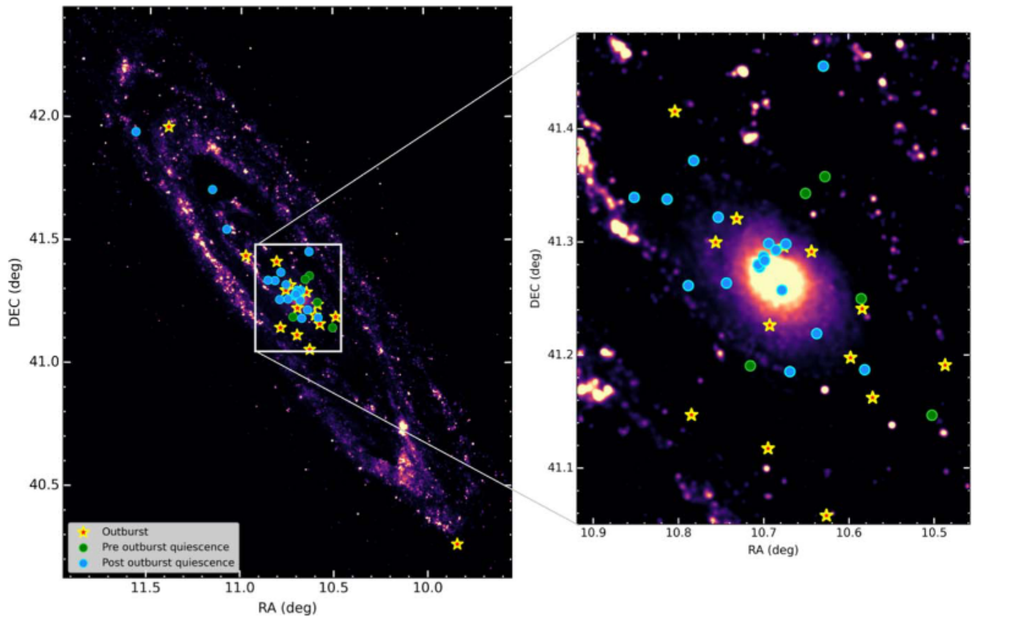

Figure 1. UVIT F148W mosaic image of M31 generated using SWarp. The locations of all the novae detected in the archival images are marked in the figure. The inset shows a zoomed-in version of the M31 central region.

DATA

2.2. Removal of Background Contribution from the Bulge

- The first method involves a median combination of multiepoch images of the same field in the same filter. Flux scaling of the multiepoch images thus only involved normalizing by their respective exposure times. Since UVIT is a space-based telescope, we expect the point-spread function (PSF) to be constant across all epochs; hence, PSF matching was not performed before combining the images. The flux-scaled images were registered and then median combined to make the template. This template was subtracted from the normalized image of each epoch to look for novae.

- In the second method, they generated an isophote model of the bulge. They modeled the bulge of M31 by performing an isophote fit using the isophote module of the photutils python package (Bradley et al. 2023). The isophote model generated for a given range of semimajor axis (~400 pixels = 2.78') for each epoch was used as a template. Subtracting this template from its original image reveals all sources above the nuclear brightness level predicted by the model.

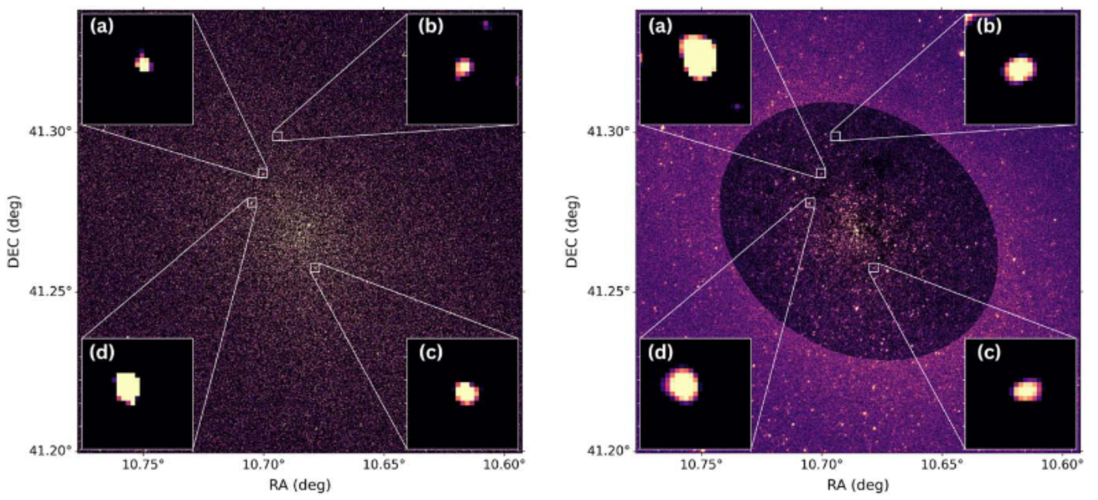

Figure 2. Difference images with inset showing detection of novae (a) M31N 2016-03e, (b) M31N 2015-05a, (c) M31N 2016-05b, and (d) M31N 2016-03c. Left: median-combined template subtraction method. Right: isophote model subtraction method.

DATA

2.3. Source Detection and Photometry

- They have detected 42 novae in various fields of M31 observed by UVIT.

PSF photometry was performed using an elliptical Moffat function to fit the sources. Standard routines in IRAF were used for photometric measurements. To accurately measure the flux, we performed aperture photometry with an aperture of 15 pixels (~4 × FWHM) and PSF photometry with a PSF radius of 11 pixels (~3 × FWHM) of isolated bright sources to determine the aperture correction term. This correction took care of the emission from the extended PSF wings. It was then applied to the magnitudes of the novae obtained by PSF photometry.

Table 2
List of M31 Novae Detected in UVIT Images and Their F148W Mag

Name M31N	R.A. (hh:mm:ss)	Decl. (dd:mm:ss)	Discovery Date (JD)	Observation Date (JD)	Mag (F148W) (AB mag)	Class (Phase)	t_2 (days)	References
Detected at Post-outburst Quiescence								
2015-02a[a]	00:42:33.06	+41:13:08.90	2457047.810	2457671.8566	23.27 ± 0.24	Fe II	⋯	(1–3)
2015-10b[a]	00:43:13.54	+41:20:16.00	2457321.400	2457671.8566	22.54 ± 0.13	Fe II	100.3 ± 75.8 (R)	(4, 5, 75)
2016-02b	00:44:37.03	+41:42:26.40	2457430.370	2457430.3700	22.01 ± 0.12	Fe II	⋯	(6)
2016-03b	00:42:19.51	+41:11:13.70	2457446.280	2457671.8567	22.16 ± 0.14	Nova	41.5 ± 7.1 (R)	(67, 68, 75)
1994-09b	00:42:58.52	+41:15:49.80	2449622.800	2457671.8566	21.88 ± 0.13	⋯	⋯	(32)
2010-12b	00:42:31.08	+41:27:20.30	2455540.620	2457671.8566	21.64 ± 0.09	⋯	3(R)[d]	(33, 34)
2013-10c	00:43:09.32	+41:15:41.60	2456574.800	2457671.8566	24.32 ± 0.30	Nova	5.5 ± 1.7 (R)	(35, 36, 75)
2015-12d	00:43:07.79	+41:22:19.30	2457387.220	2457671.8566	21.72 ± 0.10	⋯	⋯	⋯
2018-12a	00:42:40.65	+41:11:08.00	2458455.320	2458788.0143	23.31 ± 0.14	Fe II	⋯	(39–42)
2018-12d	00:43:24.62	+41:20:22.30	2458474.090	2458788.0143	23.33 ± 0.12	Nova	⋯	(42, 43)
2019-06b	00:42:41.73	+41:17:53.70	2458661.560	2458788.0143	22.75 ± 0.14	⋯	⋯	(44)
2019-07c[a]	00:43:00.90	+41:19:19.40	2458672.510	2458788.0143	21.53 ± 0.06	⋯	⋯	(45)
2019-08b	00:44:18.25	+41:32:47.20	2458725.440	2459167.9797	22.00 ± 0.08	Fe II	>57(r'), >53(g')[d]	(46, 47)
2015-05a	00:42:46.60	+41:17:55.3	2457153.56	2457671.8566	23.66 ± 0.31	Nova	⋯	(69, 70)
2019-12b	00:42:20.47	+41:15:00.00	2458833.090	2457671.8566	23.42 ± 0.25	Fe II	50(r'), 27(g')[d]	(60–62)
2021-07d	00:42:00.58	+41:08:48.30	2459420.380	2458788.0143	22.99 ± 0.13	⋯	⋯	⋯
2019-11f[b]	00:42:51.76	+41:11:26.60	2458814.160	2457671.8566	22.95 ± 0.21	⋯	⋯	(59)
2020-10b[b]	00:42:30.67	+41:21:28.50	2459127.230	2457671.8566	22.15 ± 0.13	⋯	⋯	(63, 64)
2020-10d[b]	00:42:36.20	+41:20:35.50	2459101.180	2457671.8566	23.12 ± 0.20	⋯	⋯	(65)
Detected during Outburst								
2016-08b[a]	00:41:56.82	+41:11:27.60	2457611.050	2457671.8566	20.71 ± 0.12	⋯	42.6 ± 4.3 (R)	(7, 8, 75)
2016-08e	00:43:53.29	+41:26:21.60	2457630.420	2457704.1355	20.83 ± 0.06	Fe II	60.6 ± 16.7 (R)	(9, 10, 75)
2016-09a	00:42:55.66	+41:19:14.50	2457654.300	2457671.8566	23.56 ± 0.22	Fe II	57.0 ± 35.1 (R)	(11, 12, 75)
2016-09b	00:42:17.29	+41:09:44.40	2457657.660	2457671.8566	21.18 ± 0.09	Fe II	43.9 ± 17.3 (R)	(13–15, 75)
2018-05a	00:45:34.90	+41:57:40.40	2458246.700	2458292.3095	20.84 ± 0.12	⋯	⋯	(16)
2019-11a	00:42:30.37	+41:03:29.50	2458789.760	2458805.2565	22.92 ± 0.15	Nova	49(r')[d]	(17, 18)
2020-09b	00:42:46.30	+41:13:35.50	2459117.200	2459174.7140	23.36 ± 0.18	Fe IIb	⋯	(19, 20)
2020-09c	00:43:08.38	+41:08:50.00	2459121.790	2459174.7140	21.64 ± 0.08	Fe II	17(r'), 15(g')[d]	(21, 22)
2020-10f	00:42:20.17	+41:14:28.00	2459154.530	2459174.7140	20.74 ± 0.05	Nova	⋯	(23–25)
2020-11a	00:42:46.79	+41:07:03.10	2459155.080	2459174.7140	21.82 ± 0.09	Nova	⋯	(26, 27)
2020-11c	00:43:13.15	+41:24:56.00	2459159.240	2459174.7140	19.05 ± 0.03	Fe IIb	20(r')[d]	(28–31)
2019-09b	00:42:42.32	+41:17:45.80	2458740.280	2458788.0143	21.72 ± 0.07	He/N	⋯	(48–50)
2019-10c[a]	00:43:01.56	+41:17:59.60	2458776.280	2458788.0143	21.09 ± 0.05	Fe II	18(r'), >22(g')[d]	(54–58)
2021-03a	00:42:34.49	+41:17:29.80	2459188.680	2459174.7140	22.89 ± 0.15	⋯	⋯	(66)
2018-08b	00:39:21.90	+40:15:48.80	2458344.080	2458435.0755	20.92 ± 0.10	Fe II	⋯	(37, 38)
2019-10a[c]	00:42:23.53	+41:11:52.20	2458759.300	2458788.0143	21.78 ± 0.08	Nova	>18(r'), >29(g')[d]	(51–53)

Name M31N	R.A. (hh:mm:ss)	Decl. (dd:mm:ss)	Discovery Date (JD)	Observation Date (JD)	Mag (F148W) (AB mag)	Class (Phase)	t_2 (days)	References
Detected at Post-outburst Quiescence								
2015-02a[a]	00:42:33.06	+41:13:08.90	2457047.810	2457671.8566	23.27 ± 0.24	Fe II	⋯	(1–3)

rate of decline

Table 3
Photometric Data of the UVIT-detected M31 Novae

Name M31N	R.A. (deg)	Decl. (deg)	Discovery (JD)	Observation (JD)	Δt (days)	Filter	Mag (mag)	Limit (mag)
2016-08b	10.48675	41.19100	2457611.05	2457671.85662	60.80662	F148W	20.71 ± 0.13	99
2016-08b	10.48675	41.19100	2457611.05	2457672.19496	61.14496	F172M	20.24 ± 0.22	99
2016-08b	10.48675	41.19100	2457611.05	2457671.85657	60.80657	N219M	20.76 ± 0.11	99
2016-08b	10.48675	41.19100	2457611.05	2457672.19491	61.14491	N279N	19.01 ± 0.11	99

Result and Discussion

Novae Detected at Quiescence

- Due to the wide spectrum of speed class of novae, they decided to take 100 days as the cutoff for novae in outburst, corresponding to a 7 mag decline from maxima for a 0.9 $M_\odot$ CO WD (Hachisu & Kato 2006). Additionally, considering pre-eruption dips and early UV flash, they consider novae detected within 20 days before the eruption to be in the outburst phase. For any other case, the detection is considered to be at quiescence. Twenty-three novae were detected during quiescence, 21 of which were detected post-outburst.

The light curve of nova 2019-12b (middle panel in Figure 3) shows a variability in the F148W filter, notably a dip of ~0.5 mag around 28 days before the eruption.
Zamanov et al. (2023) pointed out that dips in light curves are caused by the accumulation of an optically thick, dense shell surrounding the WD prior to the nova eruption.

Novae Detected during Quiescence and at Outburst

2019-10a was observed in the F148W filter at 46 and 415 days after the outburst, and this indicates a declining trend in its light curve.
2019-11f shows a pre-eruption dip similar to that of 2019-12b. In the F148W filter, it was observed 1140 and 8 days before the eruption and 360 days after the eruption. Additionally, the pre-eruption dip of 2019-11f is confirmed in the F172M filter observed 1140 and 8 days before the eruption.

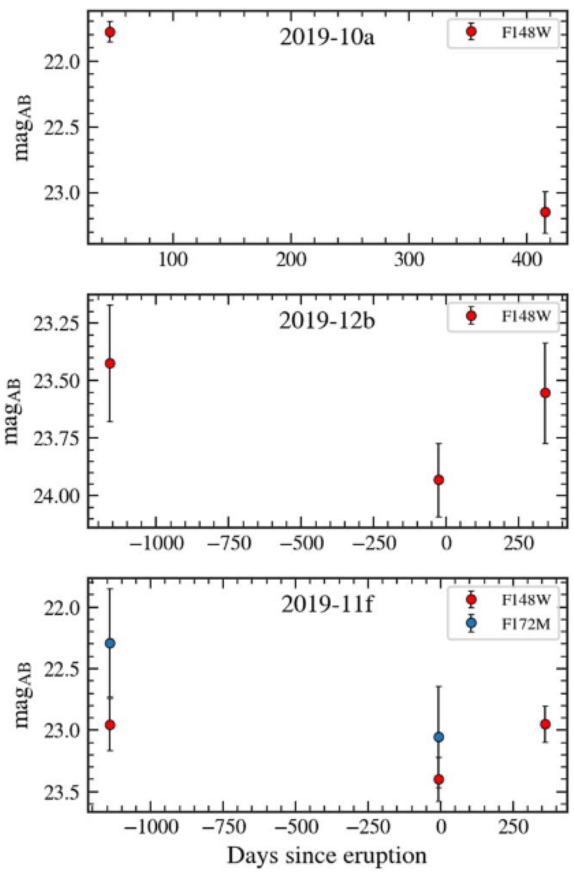

Figure 3. UVIT light curves of some interesting candidates.

Result and Discussion

The SEDs

Thirteen novae out of the 35 detected have near-simultaneous (within 2 days) observations in multiple filters in the NUV and FUV. These data sets encouraged us to look into their SEDs.

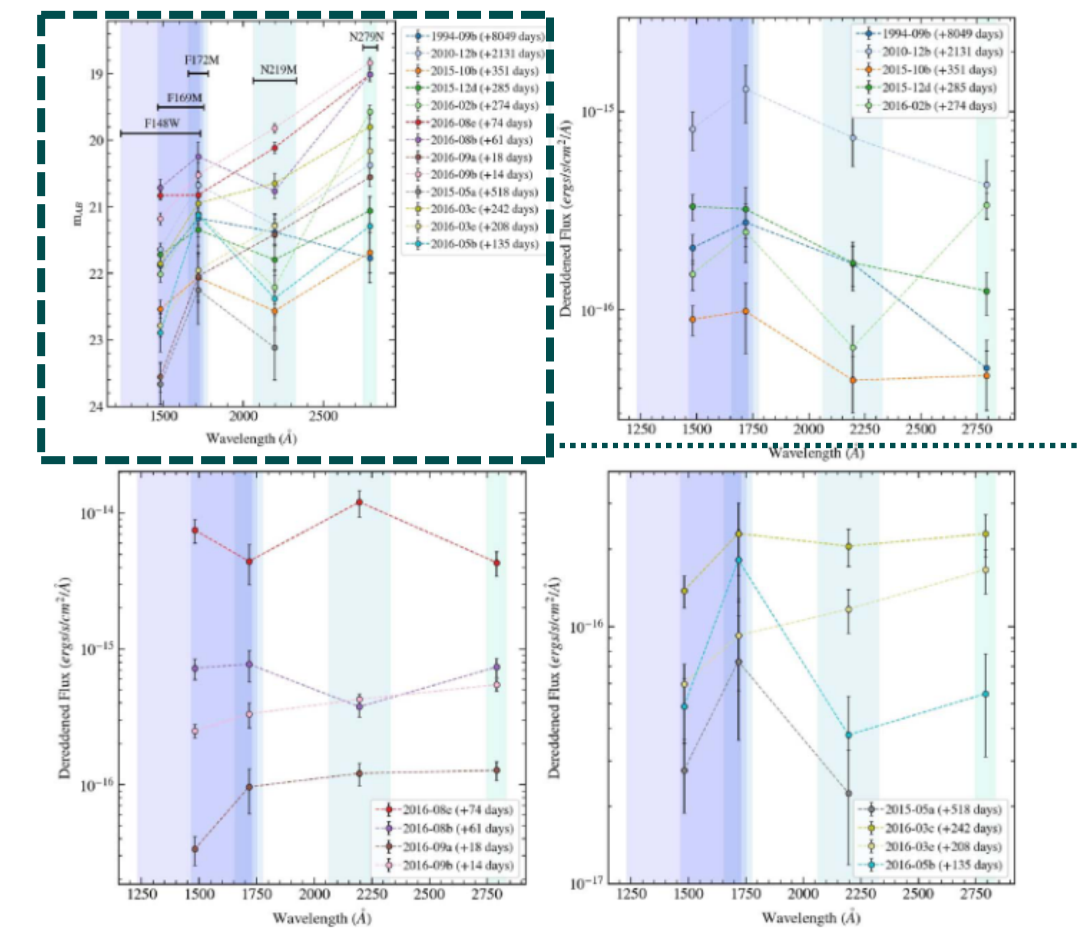

Figure 4. SED of novae detected after outburst are shown in the top-left panel with AB magnitude in the *y*-axis and wavelength in the *x*-axis. The UVIT filter bands are also marked. The extinction-corrected flux of novae detected at post-outburst quiescence (top right), detected close to outburst (bottom left), and detected in the central region (bottom right) are also shown.

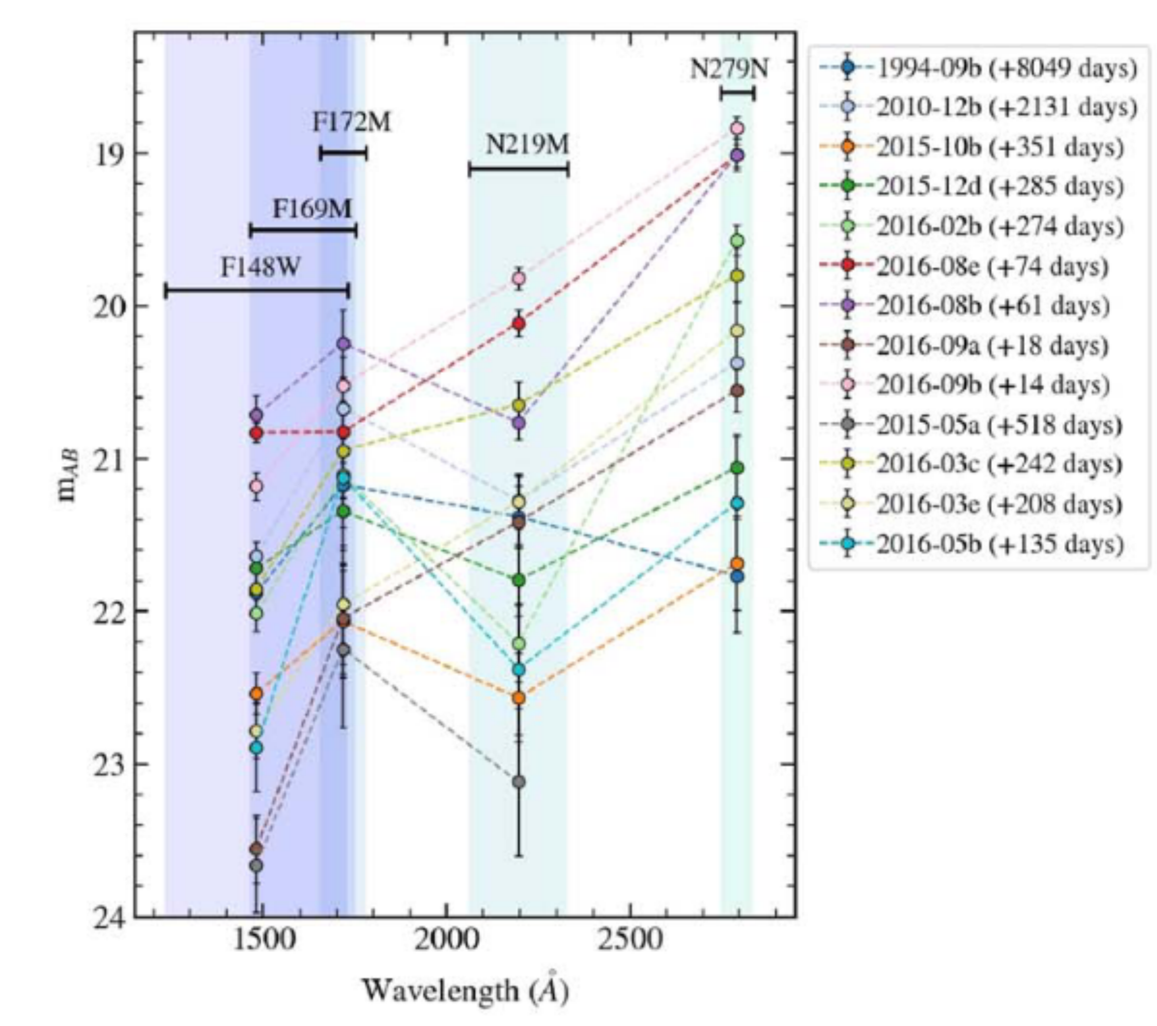

Result and Discussion

Novae were caught at post-outburst quiescence.

- The power-law dependence of $F_\lambda \propto \lambda^{-\alpha}$ was fitted to obtain the best-fit power laws given in Table 4.
- The radiation from accretion disks follows a power law with a slope of $\alpha = 7/3$. The best-fit α values for the novae are within the error bars of this, indicating the presence of accretion disks (Frank et al. 2002). This confirms that most of the UV radiation originates from the accretion disk at quiescence (Selvelli & Gilmozzi 2013).
- Another point to note is that the flux in the F148W filter is comparatively less than that in F172M. This could indicate that blueward of 1600 Å, the flux from the disk starts to diminish and could have a contribution from the WD's blackbody tail.

Table 4
α Values of Novae with Accretion Disk Signatures

M31N	α
1994-09b	2.71 ± 0.81
2010-12b	2.29 ± 0.01
2015-10b	2.01 ± 0.96
2015-12d	2.15 ± 0.33

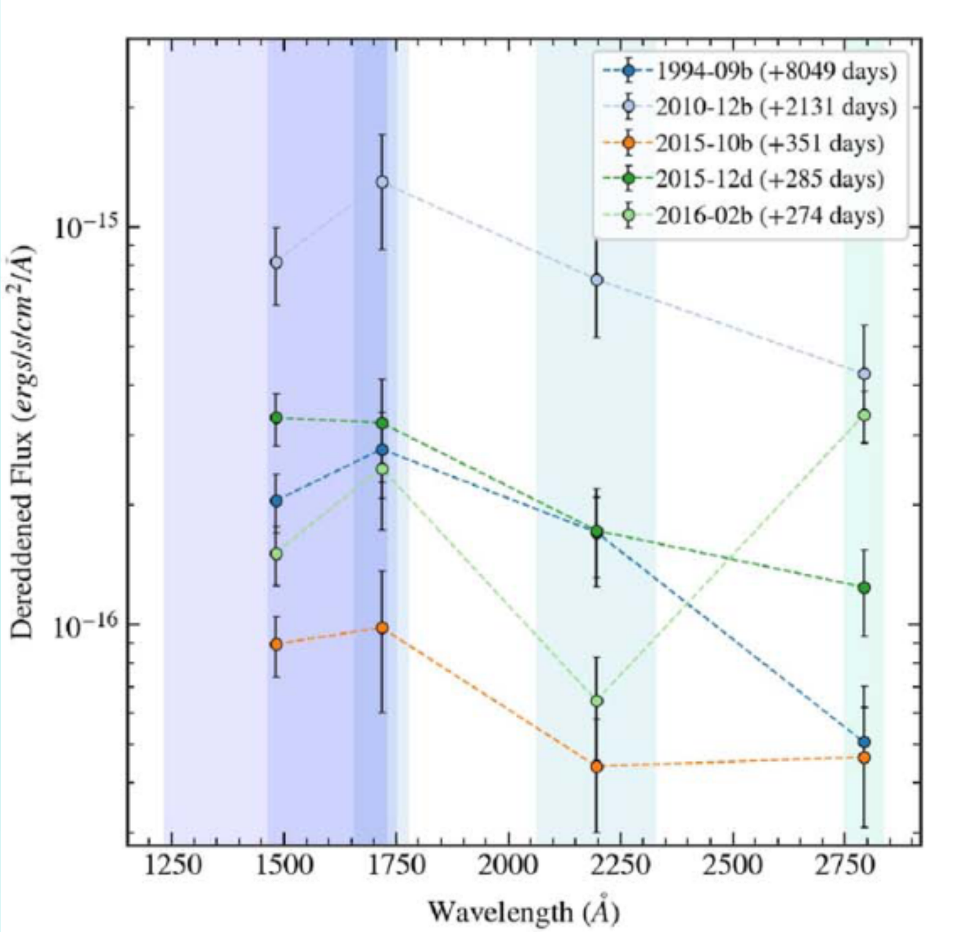

Result and Discussion

Four novae were caught during their eruption.

- Two novae, 2016-09a and 2016-09b, were observed within 18 days of eruption. Their speed class suggests that they belong to a moderately fast category, and both were also confirmed to be in their Fe II phase.
- Their SEDs indicate an increasing flux from the FUV to the NUV, hinting at the peak being in the optical region.
- The SEDs of the novae 2016-08e, and 2016-08b deviate from the power law expected from accretion disks. One possible cause for this could be the presence of spectral features in the UV bands.

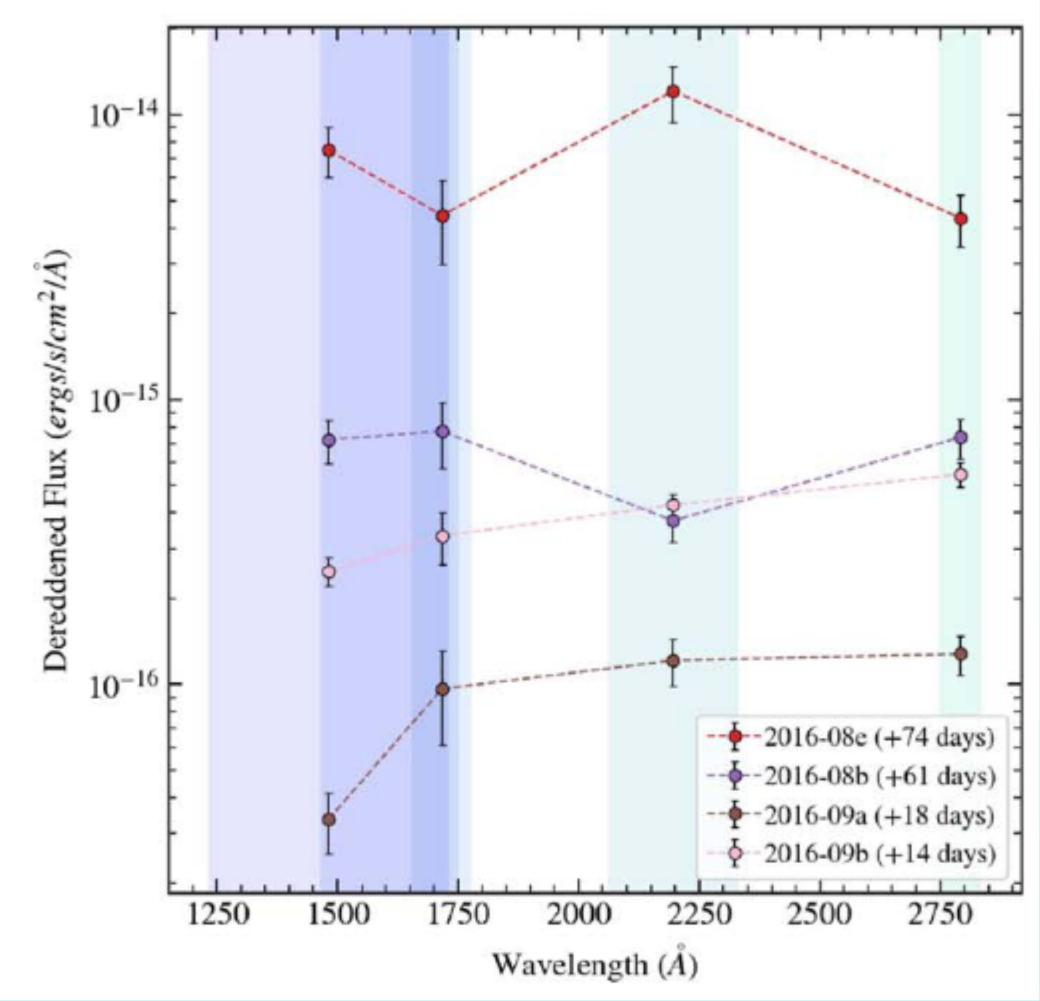

Result and Discussion

Novae were detected in the central region.

- The bulge of M31 in FUV is complicated. Leahy et al. (2023) could fit the bulge with a single component but showed that an eight-component model fits best. Such a complicated bulge region will lead to contamination, dependent on the spatial location of the novae and on the different UV wave bands.
- Furthermore, the location of these novae inside the nuclear region is unknown, leading to uncertainties in determining their column densities and extinction. It thus becomes difficult to extract much information from the SEDs of novae in the central region of M31.

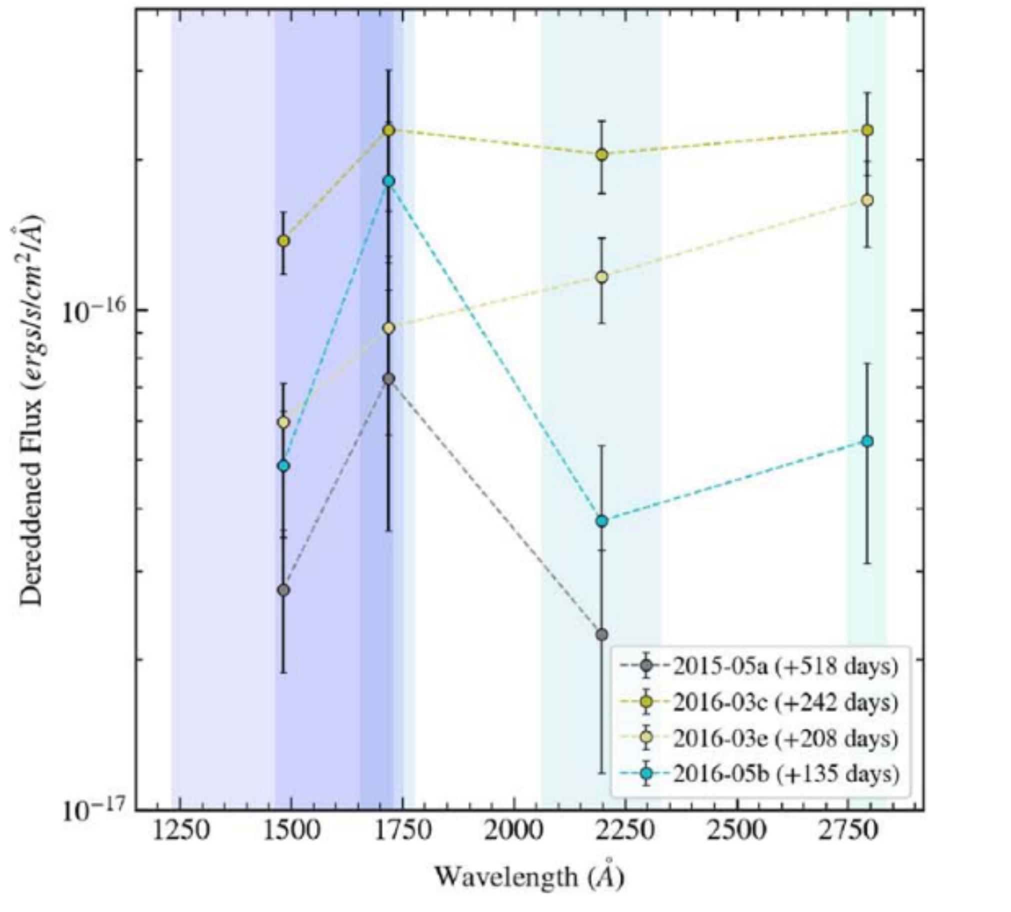

Summary and Conclusion

- 1. We have examined 91 sets of UVIT images of M31 from 2016 onward, uncovering at least one nova in 19 of those images. Over 80% of the identified novae were situated within or close to the central bulge.
- 2. We employed two image subtraction methods to eliminate the light from the galactic bulge, leading to the detection of four novae previously obscured by the brightness of the central region of M31.
- 3. A total of 42 novae were identified, with 15 observed across multiple filters in both the FUV and the NUV. Additionally, several novae were detected in multiple epochs. Magnitude upper limits were estimated for more than 1000 novae undetected in individual and coadded frames.
- 4. During quiescence, the SEDs of novae exhibit indications of the accretion disk's influence, confirming its dominance in UV radiation during this phase. Analysis of the SEDs of two novae during outburst indicates they were observed while their photospheres were receding.
- 5. The FUV light curves of two novae exhibit a pre-eruption dip that can possibly be attributed to the accumulation of accreted material in a shell before the nova eruption. Multiepoch photometry of the novae at quiescence indicates a near-constant magnitude, a sign of a steady accretion rate.

THANKS!